

PARALLEL R-CENTIPEDES

Fast Contour Extraction for 3D Visualization

Mehdi Nouri Shirazi and Yoshiyuki Kamakura

Faculty of Information Science and Technology, Osaka Institute of Technology, Osaka, Japan

Keywords: Deformable Contours, Active Contours, Electron-microscope Tomographic Images, 3D-visualization.

Abstract: In our previous article, we introduced a class of region-based deformable contour models called R-centipedes. The R-centipedes are able to operate in three modes: 1) deflationary, 2) inflationary, or 3) a mixture of both. We demonstrated that the deflationary R-centipedes could adaptively change their structures in order to extract structures of interest and their substructures from complex Electron Microscope (EM) tomography slice images. The R-centipedes have several desirable features such as 1) structural flexibility which allows them to extract multiple objects in a single slice image, 2) high accuracy, and 3) insensitivity with respect to their initial positions and configurations. In this article, we introduce two parallel versions of the R-centipedes, 1) implicit, and 2) explicit parallel R-centipedes. We present three simulation studies to demonstrate their flexibility, effectiveness and computational efficiency in extracting structures in three different complex situations.

1 INTRODUCTION

Extracting meaningful structures of interest and their internal structures from medical and EM tomographic slice images for 3D visualization is a challenging problem. This is due to the complexity and variability of the biological structures that are usually embedded in intensity inhomogeneities, imaging noise, textural artifacts and boundary irregularities, the large size ($> 1000 \times 1000$ pixels) and numerous number (> 256 slices) of tomographic images that should be processed. The challenge is to extract the boundary pixels belonging to the structures of interest from each slice image and integrate them into complete and consistent 3D representations of the objects and their parts as fast as possible and preferably with no or minimal user interaction.

Deformable contour models (McInerney and Terzopoulos, 1996), including the standard energy-minimizing snakes (Kass et al., 1988) and balloons (Cohen, 1991), offer an attractive approach to contour extraction problem and have been used broadly in image segmentation. The active contours move and deform within the slice images under a combined influence of internal and external forces.

Though the standard deformable models have proved to be very useful tools in 3D visualization they suffer from some characteristic limitations. First, they should manually be initialized close to the boundaries

of the target objects. Second, the segmentation results might be dependent on the positions of the initial contours. Third, they are geometrically inflexible due to inability to re-parametrize. Finally, they are incapable of adapting to object topology.

To overcome the limitations of the standard snakes, McInerney and Terzopoulos (McInerney and Terzopoulos, 1995) augmented the snakes with re-parametrization, splitting and merging mechanisms using the affine cell image decomposition (ACID) technique. They showed that their topology adaptive snakes, called the T-snakes, could successfully extract multiple objects and even grew into structures with complex geometries in different medical image analysis scenarios.

Almost all the standard explicit snakes and their topology adaptive versions are edge-based models. There are several well known problems with edge-based snakes. First, edge-based snakes use edge detector to stop their evolving contours on the boundaries of the target objects. Second, if the image is noisy, the image should be smoothed isotropically. If the image is very noisy, the Gaussian smoothing has to be strong which will smooth the stopping edges too. Third, to get rid of spurious weak edges the user has to set a threshold, which is usually a critical parameter that directly affects the quality of the segmentation result. Fourth, the edge-based models are inapplicable in cases where the boundaries of the

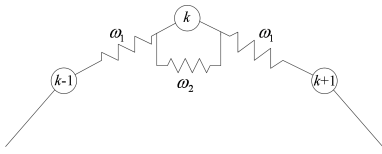


Figure 1: The neighboring nodes of a closed centipede are coupled through the elasticity and rigidity parameters, ω_1 , ω_2 .

target objects are not necessarily defined by gradients. Fifth, they easily get stuck with textural artifacts.

These limitations seriously mitigate the applicability of the edge-based snakes in complex situations in general, and in EM tomography image analysis and 3D visualization in particular, where demands are high for speed, accuracy and automation with no or minimal user interaction.

In our previous article (Shirazi and Kamakura, 2010), we introduced a class of region-based topologically flexible deformable models that we called restructuring centipedes (R-centipedes). In this article, we introduce two parallel versions of the R-centipedes dubbed explicit parallel R-centipedes and implicit parallel R-centipedes. Our experiments with the parallel R-centipedes have shown that they are structurally flexible enough: 1) to extract structures with complex boundaries from EM tomography slice images when operating in their deflationary mode, and 2) grow into micro-tubular complex structures with high speed and accuracy when operating in their inflationary mode.

2 RESTRUCTURING CENTIPEDES

A closed centipede consists of a number of self-powered two-legged moving automatons (nodes), where the neighboring nodes are coupled as shown in Fig. 1. The legs are facilitated with sensory patches whereby the centipedes can interact with their environments.

Restructuring centipedes (R-Centipedes) are deformable centipedes which can restructure themselves by, 1) recruiting new nodes, 2) removing nodes, 3) splitting into new R-centipedes, and 4) merging with the other R-centipedes that they might come into contact.

As shown in Fig. 2, with each node there are associated, 1) one inner patch $P_{i,k}$, 2) one outer patch $P_{o,k}$, and 3) a self-powered moving force $\vec{\gamma}_k$.

While R-centipedes undergo deformation and restructuring, their nodes are assumed to keep the axes of their inner and outer patches aligned and perpen-

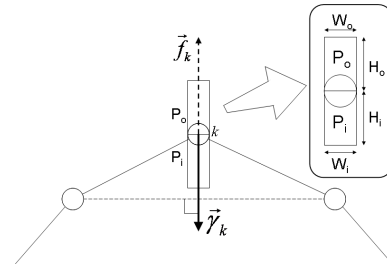


Figure 2: The inner patch $P_{i,k}$, outer patch $P_{o,k}$, self-powered moving force $\vec{\gamma}_k$, and the external force \vec{f}_k at node k .

dicular to the lines passing through their two neighboring nodes, as shown in Fig. 2.

2.1 Deformation Equations

Let $\vec{v}_k(t) = [x_k(t) \ y_k(t)]^T$ denote the time-varying position vector of node k . The dynamical behavior of a closed deformable centipede that consists of N coupled self-powered moving nodes is assumed to be governed by the following motion equations

$$\dot{\vec{v}}_k - \vec{\alpha}_k + \vec{\beta}_k - \vec{\gamma}_k = \vec{f}_k, \quad (1)$$

for all $k = 0, \dots, N-1$. The first term of Eq. (1), $\dot{\vec{v}}_k$, denotes the velocity of node k , $\vec{\alpha}_k$ and $\vec{\beta}_k$ are image-independent internal forces known as the tensile force and the flexural force at node k , respectively, $\vec{\gamma}_k$ is a self-powered moving force at node k , and finally \vec{f}_k is an external force which the image might exert at node k .

The internal tensile and flexural forces are given by

$$\vec{\alpha}_k(t) = \omega_1 \Delta^2 \vec{v}_k(t), \quad (2)$$

and

$$\vec{\beta}_k(t) = \omega_2 \Delta^2 (\Delta^2 \vec{v}_k(t)), \quad (3)$$

respectively, where the 2nd-order difference operator Δ^2 is given by

$$\Delta^2 \vec{v}_k(t) = (\vec{v}_{k-1}(t) - 2\vec{v}_k(t) + \vec{v}_{k+1}(t)) / (\Delta l(t))^2. \quad (4)$$

In the above equations, the parameter ω_1 controls the resistance of the centipede to expanding and/or shrinking, whereas ω_2 controls the resistance of the centipede to bending at its nodes, and finally $\Delta l(t)$ denotes the time-varying distance between the immediate neighboring nodes. For closed centipedes, all indexes in the above expressions is interpreted modulo N .

The self-powered moving forces are given by

$$\vec{\gamma}_k(t) = c_\gamma \vec{n}_k(t), \quad (5)$$

where $\vec{n}_k(t)$ denotes a time varying vector defined as a unit vector perpendicular to the line passing through the k -th node's immediate two neighboring nodes. The constant c_γ controls the magnitude of the self-powered forces. When all nodal self-powered forces are exerted inwardly the R-centipede shrinks (deflationary R-centipede), when all exerted outwardly it expands (inflationary R-centipede), and when partly inwardly and partly outwardly we will have deflationary/inflationary R-centipedes which can be used in object tracking problems.

The last components which affect the behaviors of R-centipede are the time-varying external forces $\vec{f}_k(t)$. The concrete form of these forces are in general application dependent. Here, we define them as image-dependent stopping forces which can eventually bring the deformation process to halt at the boundaries of the objects of interest.

Let $P_{i,k}(t)$, and $P_{o,k}(t)$ denote the sets of the locations of the pixels that come under the inner and outer patches of node k at time t , respectively. Let $m_{i,k}(t)$ and $m_{o,k}(t)$ denote the mean values of the gray-levels of the pixels belong to $P_{i,k}(t)$, and $P_{o,k}(t)$, respectively, by

$$m_{i,k}(t) = \frac{1}{|P_{i,k}(t)|} \sum_{(i,j) \in P_{i,k}(t)} I(i,j), \quad (6)$$

$$m_{o,k}(t) = \frac{1}{|P_{o,k}(t)|} \sum_{(i,j) \in P_{o,k}(t)} I(i,j), \quad (7)$$

where $|P_{i,k}(t)|$, and $|P_{o,k}(t)|$ are the cardinal numbers of $P_{i,k}(t)$ and $P_{o,k}(t)$, respectively.

Furthermore, let $\bar{m}_i(t)$ and $\bar{m}_o(t)$ denote the means of $m_{i,k}(t)$ and $m_{o,k}(t)$ and $\sigma_i(t)$ and $\sigma_o(t)$ their standard deviations. Then, the external nodal forces for the deflationary R-centipedes are defined by

$$\vec{f}_k(t) = \begin{cases} -\vec{\gamma}_k(t), & \text{if } m_{i,k}(t) \geq \bar{m}_o(t) + c_s \sigma_o(t) \\ 0, & \text{otherwise,} \end{cases} \quad (8)$$

and for the inflationary R-centipedes by

$$\vec{f}_k(t) = \begin{cases} -\vec{\gamma}_k(t), & \text{if } m_{o,k}(t) \leq \bar{m}_i(t) + c_s \sigma_i(t) \\ 0, & \text{otherwise.} \end{cases} \quad (9)$$

Here the constant c_s controls the degree of textural mismatching that is tolerated, and t_0 denotes the time when the R-centipede is created and set free to move and deform.

2.2 Restructuring Rules

The R-centipedes are allowed to restructure by, 1) recruiting (adding) new nodes, 2) dismissing (deleting) nodes, and 3) splitting. They add and delete nodes in

order to keep the lengths of their two-node segments approximately constant. They check the lengths of their segments after each incremental deformation, add a new node in the middle of any segment which they find to be too long, and/or delete one of the two nodes of any segment which they find to be too short. Active R-centipedes are also allowed to split into two R-centipedes whenever they detect a self-crossing.

The ability to split enable the R-centipedes, firstly, to generate the same final configurations regardless of their initial positions/configurations that encompass the objects of interest, secondly, to extract multiple objects in slice images, and thirdly, not get stuck with textural artifacts which exist rampantly in EM tomography slice images.

2.3 Non-parallel Incremental Deformation Rule

To solve the motion equations of a deflationary R-centipede defined by Eqs. (1)-(6) and (8), or an inflationary R-centipede defined by Eqs. (1)-(7) and (9), we used the implicit Euler method in our previous article (Shirazi and Kamakura, 2010). The implicit Euler method approximates the temporal derivatives with forward finite differences. It updates the x- and y-components of the positions of nodes from time t to time $t + \Delta t$ according to the following $2N$ system of nonlinear equations

$$(I + \Delta t C(t)) \vec{V}(t + \Delta t) = \vec{V}(t) + \Delta t (\vec{F}(t) + \vec{\Gamma}(t)), \quad (10)$$

where I denotes the $(N(t) \times N(t))$ -dimensional identity matrix, whereas $C(t)$ denotes an $(N(t) \times N(t))$ -dimensional matrix known as the stiffness matrix (for detail, see (Shirazi and Kamakura, 2010)).

In the above equation, $\vec{V}(t) = [\vec{v}_0(t) \dots \vec{v}_{N(t)-1}(t)]^T$ denotes the $N(t)$ -dimensional vectors of the locations of the centipede's nodes at time t , whereas $\vec{\Gamma}(t) = [\vec{\gamma}_0(t) \dots \vec{\gamma}_{N(t)-1}(t)]^T$ denotes the $N(t)$ -dimensional vectors of the self-powered moving nodal forces, and $\vec{F}(t) = [\vec{f}_0(t) \dots \vec{f}_{N(t)-1}(t)]^T$ denotes the the image-dependent stopping forces at time t .

3 PARALLEL INCREMENTAL DEFORMATION RULES

By expanding Eq. (1) at the node k , and by using Eqs. (2)-(4) we will get

$$\begin{aligned} \dot{\vec{v}}_k &= \vec{f}_k + \vec{\gamma}_k \\ &- c_2 \vec{v}_{k-2} - c_1 \vec{v}_{k-1} - c_0 \vec{v}_k \\ &- c_1 \vec{v}_{k+1} - c_2 \vec{v}_{k+2}. \end{aligned} \quad (11)$$

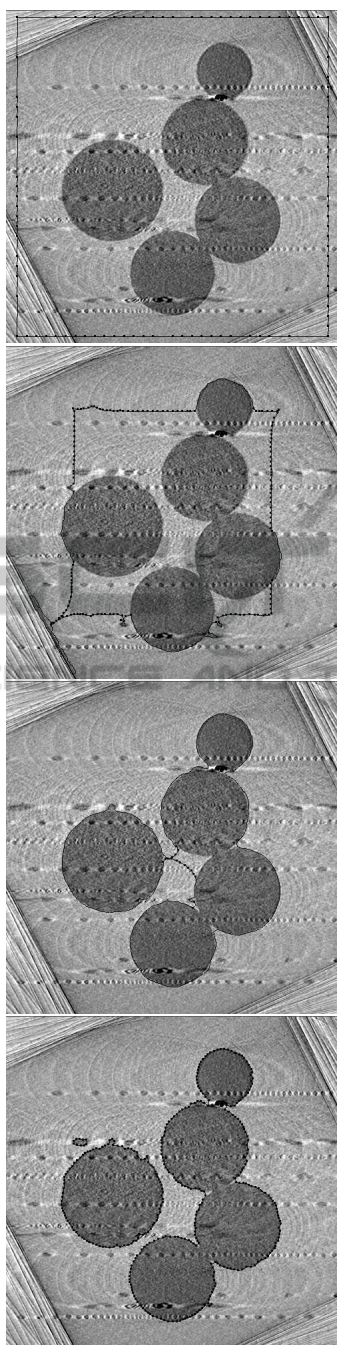


Figure 3: Deflationary mode: snap shots of the contour extraction process. The bottom image shows the final positions/configurations of the four R-centipedes that generated and survived in the process.

where c_0 , c_1 and c_3 are given as

$$c_0 = \frac{2\omega_1}{(\Delta l(t))^2} + \frac{6\omega_2}{(\Delta l(t))^4}, \quad (12)$$

$$c_1 = -\frac{\omega_1}{(\Delta l(t))^2} - \frac{4\omega_2}{(\Delta l(t))^4}, \quad (13)$$



Figure 4: Inflationary mode: snap shots of the contour extraction process. The bottom image shows the extracted boundary of a clicked substructure of an alga.

$$c_2 = \frac{\omega_2}{(\Delta l(t))^4}. \quad (14)$$

By using the implicit Euler method we can discretize Eq. (11) in time domain and get

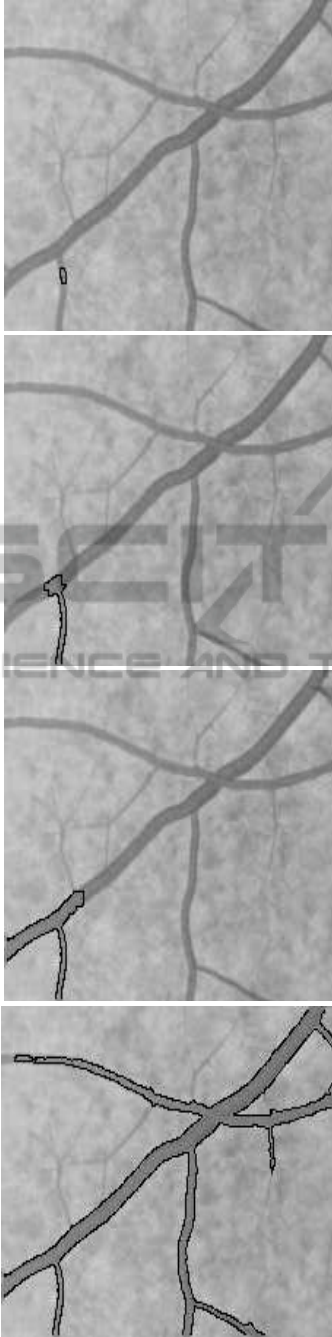


Figure 5: Inflationary mode: snap shots of the extraction process. The bottom image shows the extracted boundary of a micro-tubular structure.

$$\begin{aligned}
 (1 + \Delta t c_0) \vec{v}_k(t + \Delta t) &= \vec{v}_k(t) \\
 &- (c_2 \vec{v}_{k-2}(t) + c_1 \vec{v}_{k-1}(t) \\
 &+ c_1 \vec{v}_{k+1}(t) + c_2 \vec{v}_{k+2}(t)) \Delta t \\
 &+ (\vec{f}_k(t) + \vec{\gamma}_k(t)) \Delta t, \quad (15)
 \end{aligned}$$

and by using the explicit Euler method we get

$$\begin{aligned}
 \vec{v}_k(t + \Delta t) &= (1 - \Delta t c_0) \vec{v}_k(t) \\
 &- (c_2 \vec{v}_{k-2}(t) + c_1 \vec{v}_{k-1}(t) \\
 &+ c_1 \vec{v}_{k+1}(t) - c_2 \vec{v}_{k+2}(t)) \Delta t \\
 &+ (\vec{f}_k(t) + \vec{\gamma}_k(t)) \Delta t. \quad (16)
 \end{aligned}$$

The rules given by the updating Eqs. (15) and (16) are two different parallel versions of the non-parallel incremental deformation rule given by the updating rule (10).

4 SIMULATION EXPERIMENTS

4.1 Experiment 1

We applied the deflationary non-parallel and the two parallel R-centipedes to the 500×500 test EM slice image shown in Fig. 3. We initiated 4-node R-centipedes and positioned them near the frame of the test image and let them move, deform, split and adapt their nodes until they stabilized and stopped. The upper three images show the snap shots of the intermediate positions and configurations of the deflationary implicit parallel R-centipede at three different instances. Though the intermediate positions and configurations of the non-parallel and explicit parallel R-centipedes were different, their final configurations were almost the same to such extend that we decided not to put them here for the sake of space. We used the same parameters for the non-parallel and parallel R-centipedes. The parameters used in the simulation were: $\omega_1 = 0.2$, $\omega_2 = 0.4$, $\gamma_c = 300$, $c_s = 2.5$, $H_o = H_i = 4$ (pixels), $W_o = W_i = 7$ (pixels), $\Delta l(t) = \Delta l = 5$ (pixels), and $\Delta t = 0.01$.

This experiment clearly shows that, regardless of the numerous textural artifacts scattered over the background, the parallel R-centipedes like their non-parallel predecessor are able to extract the contours of the objects of interest with high precision.

The cpu-time that the non-parallel R-centipede used was 6.18 seconds, while the two parallel R-centipedes used about 1.93 seconds each.

4.2 Experiment 2

In our second experiment designed to demonstrate the effectiveness and the speed of the proposed inflationary parallel R-centipedes, we applied the non-parallel and parallel R-centipedes to the 512×512 EM slice image of an alga shown in Fig. 4.

The R-centipedes were initiated by a mouse click on the internal substructure of interest and were let

free to move, deform, split and adapt their nodes until they stabilized and stopped.

The three upper images of Fig. 4 show the intermediate positions/configurations of the implicit parallel R-centipede at different instances, whereas the bottom image shows the result of the contour extraction process. Black dots in the intermediate images show the R-centipede's active nodes, that is, the nodes which have not yet encounter the substructure's boundary and thus are still free to move. The parameters used in the simulation were: $\omega_1 = 0.02$, $\omega_2 = 0.04$, $\gamma_c = -50$, $c_s = 2.5$, $H_o = H_i = 2$ (pixels), $W_o = W_i = 7$ (pixels), $\Delta l(t) = \Delta l = 4$ (pixels), and $\Delta t = 0.01$.

The cpu-time that the non-parallel R-centipede used was 1.59 seconds, whereas the parallel R-centipedes used about 0.92 seconds each.

4.3 Experiment 3

On the contrary to the non-parallel R-centipedes which consume the cpu-time to invert the $N(t) \times N(t)$ stiffness matrices for updating the locations of all nodes, the implicit and explicit parallel R-centipedes are free from such matrix inversions and use the cpu-time for updating the locations of the active nodes only. This can make a big difference in terms of the cpu-time consumptions in cases where the inflationary R-centipedes should grow into tree-like structures with lots of branches.

To demonstrate the cpu-time consumption efficiency, in other words, to compare the speeds of the inflationary non-parallel and parallel R-centipedes, we applied them to the micro-tubular structure in the 228×177 shown in Fig. 5. The parameters used in the simulation were: $\omega_1 = 0.02$, $\omega_2 = 0.04$, $\gamma_c = -50$, $c_s = 2.5$, $H_o = H_i = 2$ (pixels), $W_o = W_i = 7$ (pixels), $\Delta l(t) = \Delta l = 4$ (pixels), and $\Delta t = 0.01$.

The cpu-time that the non-parallel R-centipede used was 81.27 seconds, whereas the parallel R-centipedes used about 9.93 seconds each.

5 CONCLUSIONS

We introduced two parallel R-centipedes, namely, the implicit parallel R-centipedes and the explicit parallel R-centipedes. Our simulation studies have shown that they are almost identical in all situations in terms of speed and accuracy in extracting structures of interest. The parallel R-centipedes, like their non-parallel predecessor, can be used with ease to automate the labor-intensive and time-consuming contour extraction process of the 3D visualization of the objects of interest

from a large number of medical and EM tomography slice images with minimal user interaction.

ACKNOWLEDGEMENTS

This research was carried out in cooperation with the Research Center for Ultra-High Voltage Electron Microscopy of Osaka University and was supported by a grant from JST (Japan Science and Technology Agency).

REFERENCES

- Cohen, L. D. (1991). n active contour models and balloons. *CVGIF: Image Understanding*, 53(2):211–218.
- Kass, M., Witkin, A., and Terzopoulos, D. (1988). Snakes: active contour models. *Int. J. Comp. Vision*, 1(4):321–331.
- McInerney, T. and Terzopoulos, D. (1995). Topologically adaptable snakes. In *Proc. Fifth International Conference on Computer Vision (ICCV'95)*, pages 840–845.
- McInerney, T. and Terzopoulos, D. (1996). Deformable models in medical image analysis: A survey. In *Med. Image Anal.*, volume 1.
- Shirazi, M. N. and Kamakura, Y. (2010). Restructuring centipedes and their applications to fast extraction of structures in electron microscope tomography images. In *3rd International Conference on Biomedical Engineering and Informatics*.